Beamforming optimization of wideband MISO systems in the presence of mutual coupling

Sandy Saab
The University of Texas at Austin, USA
Email: shs18@utexas.edu

Amine Mezghani
University of Manitoba, Canada
Email: amine.mezghani@umanitoba.ca

Robert W. Heath Jr.
North Carolina State University, USA
Email: rwheath2@ncsu.edu

***Abstract*—We introduce a mutual information based optimization for a two-port multiple-input single-output (MISO) antenna system. We develop a complete circuit-level analysis of a compact MISO system in the wideband regime. We design a physically realizable antenna array and study the impact of mutual coupling on the spectral efficiency. Then, we maximize the system's mutual information by optimizing the beamformer under two different power constraints, namely the total dissipated power and the available power of the amplifiers. By varying the inter-element antenna spacing, we present results for the achievable spectral efficiency under different power amplifier constraints.**

***Index Terms*—Mutual Coupling, Multi-band, Beamforming, MISO, Optimization, Wideband Antenna Array.**

I. Introduction

Multiple-input multiple-output (MIMO) systems for the post-5G era (in both sub-6GHz, mmWave) are expected to be super-wideband (i.e., several octaves of bandwidth) [1]. This will enable simultaneous operation at different frequency bands for multi-connectivity (i.e., multi-radio technology) and widely-spaced carrier aggregation.

A common problem that arises when designing broadband antenna arrays is mutual coupling. The strong electromagnetic interaction between the elements can change the radiation pattern associated with each element [2]. Prior studies present interesting results on the impact of mutual coupling in compact narrowband antenna systems. While some researches claim that mutual coupling can improve the channel's mutual information by achieving pattern diversity [3], others showed that the mutual coupling can lead to impedance mismatch and spatially correlated noise [4]. Hence, the work in [5] intended to reduce mutual coupling in antenna arrays by using robust adaptive beamforming algorithms. Other researchers, however, tried to reduce mutual coupling through neutralization lines [6] and electromagnetic band-gap structures [7]. Another line of work focused on mutual coupling modeling from a circuit perspective in narrowband MIMO systems [8]. The impact of multi-element antenna arrays on the mutual information, diversity order, and the system's degree of freedom was addressed in [9], [10]. In [10] multi-port decoupling networks were used to improve the system performance in the narrowband case.

The previous work, however, focuses on narrowband antenna array systems which is not an adequate assumption for future wireless systems. In this paper, we design a compact wideband MISO system and evaluate its achievable rate in the presence of mutual coupling. The objective of our work includes a circuit-level based analysis of a two-port MISO setup. In our prior work, [11], we evaluated the achievable rate of a wideband single-input multiple-output (SIMO) system while quantifying the noise correlation matrix. In this work, we use similar channel models while exploring the transmit beamforming capabilities. We present a physically consistent antenna model to mimic a realistic behavior in the wideband regime. A challenging aspect of our analysis is finding the optimal beamformer while accounting for mutual coupling.

We begin by extracting the impedance matrix of the designed antenna array to formulate an equivalent channel model. Then, we find the optimal beamformer while accounting for a dissipated power constraint. In comparison, we evaluate the spectral efficiency while having constraints on the available power of the power amplifiers. Finally, we provide results for the spectral efficiency of these two scenarios while varying the inter-element spacing of the considered antenna array.

II. System model and problem formulation

Fig. 1 considers a MISO communication system with two transmitting antennas. The transmitter is composed of two

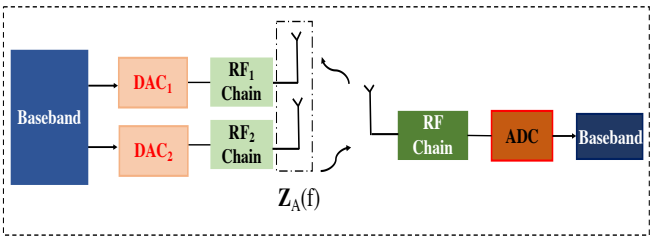

Fig. 1: MISO system model composed of 2 Tx antennas and a single receive antenna.

RF chains with separate power amplifiers. To model the circuit behavior of the MISO system, we design a two-port antenna array using Ansys HFSS software [12]. We extract from this physically realizable antenna structure the frequency dependent impedance matrix $\boldsymbol{Z}_{\mathrm{A}}(f)$. The self-impedances

are diagonal elements while mutual impedances are the off-diagonal elements

$$\boldsymbol{Z}_{\mathrm{A}}(f) = \begin{bmatrix} z_{11}(f) & z_{12}(f) \\ z_{21}(f) & z_{22}(f) \end{bmatrix}. \tag{1}$$

The off-diagonal elements are the mutual coupling indicators. When mutual coupling is severe, $z_{12}(f)$ and $z_{21}(f)$ will not be negligible (c.f. Section III). If the inter-element antenna spacing is $\leq \frac{\lambda}{2}$, mutual coupling manifests with $\lambda = \frac{c}{f}$, where f is the frequency of operation, $c = 3.10^8$m/s is the speed of light.

A. Effective channel model

The composed effective channel model, $\boldsymbol{h}_{\mathrm{eff}}(f)$, fundamentally considers in its definition the antenna array's impedance matrix $\boldsymbol{Z}_{\mathrm{A}}(f)$ and the output impedance of the power amplifiers R_{in} (e.g. $R_{\mathrm{in}} = 50\Omega$). It also includes the propagation channel $\boldsymbol{h}_{\mathrm{prop}}(f)$. The propagation channel model can be line-of-sight (LoS), rich scattering, sparse channel model, etc.. The resulting effective channel including the antenna coupling effects is

$$\boldsymbol{h}_{\mathrm{eff}}(f) = 2(\boldsymbol{Z}_{\mathrm{A}}(f)+R_{\mathrm{in}}\mathbf{I})^{-1}\sqrt{R_{\mathrm{in}}\Re(\mathrm{diag}(\boldsymbol{Z}_{\mathrm{A}}(f))}\boldsymbol{h}_{\mathrm{prop}}(f). \tag{2}$$

To derive (2), we calculate the current across the antenna terminals for a given excitation current vector $\boldsymbol{i}_{\mathrm{s}}(f)$

$$\boldsymbol{i}_{\mathrm{A}}(f) = (\boldsymbol{Z}_{\mathrm{A}}(f) + R_{\mathrm{in}}\boldsymbol{I})^{-1}R_{\mathrm{in}}\boldsymbol{i}_{\mathrm{s}}(f). \tag{3}$$

The excitation current vector is applied via a frequency dependent beamforming vector $\boldsymbol{b}(f)$ and the transmitted signal $x(f)$

$$\boldsymbol{i}_{\mathrm{s}}(f) = \frac{2}{\sqrt{R_{\mathrm{in}}}}\boldsymbol{b}(f)x(f). \tag{4}$$

Consequently, we use (3) and (4) to determine $\boldsymbol{h}_{\mathrm{eff}}(f)$ as given in (2). Note that the current vector, $\boldsymbol{i}_{\mathrm{s}}(f)$, is the vector that is controlled form the digital side, which is resulting from the space-time processing of the signal $x(f)$. In addition, only for the uncoupled case, i.e. $\boldsymbol{Z}_{\mathrm{A}} = R_{\mathrm{in}}\mathbf{I}$, we get $\boldsymbol{h}_{\mathrm{eff}}(f) = \boldsymbol{h}_{\mathrm{prop}}(f)$.

B. MISO optimal beamformer

In a MISO communication system, our main objective is finding the optimal frequency-dependent beamforming vector that maximizes the spectral efficiency of a wideband system. Accordingly, the system's input-output relationship is

$$y(f) = \boldsymbol{h}_{\mathrm{eff}}(f)^{\mathrm{T}}\boldsymbol{b}(f)x(f) + \eta(f) \tag{5}$$

where $\eta(f)$ corresponds to the noise at the receiver that follows a complex Gaussian distribution with power spectral density N_0N_{F} with N_{F} being the noise figure of the receiver. In this section, we present two different constraints that maximize the system's spectral efficiency. The first approach optimizes $\boldsymbol{b}(f)$ while having the $L2$ norm as a conventional constraint on the beamforming vector. This constraint defines an upper bound for the current sources of each power amplifier in the RF chain, i.e., the maximum available power. The second approach, however, has a constraint on the power dissipated by the current sources.

To find the optimal beamformer, we set up the optimization problem using a power constraint E with impedance kernel matrix $\boldsymbol{G}$

$$\max_{\boldsymbol{b}(f)} |\boldsymbol{h}_{\mathrm{eff}}(f)^{\mathrm{T}}\boldsymbol{b}(f)|^2 \quad \text{s.t. } \boldsymbol{b}(f)^*\boldsymbol{G}\boldsymbol{b}(f) \leq E. \tag{6}$$

The matrix $\boldsymbol{G}$ is required to define a valid power quantity based on the excitation current vector in (4) which is related to the beamforming vector. $\boldsymbol{G}$ can be for instance the identity matrix, when the constraint is the $L2$ norm corresponding to a limitation on the available power from the amplifiers. If one limits the total dissipated power by the excitation current sources $\boldsymbol{i}_{\mathrm{s}}(f)$, then $\boldsymbol{G}$ is given by

$$\begin{aligned}\boldsymbol{G} = \; & 4(\boldsymbol{Z}_{\mathrm{A}}(f)+R_{\mathrm{in}}\mathbf{I})^{-1}\left(\Re(\boldsymbol{Z}_{\mathrm{A}}(f))R_{\mathrm{in}} + \boldsymbol{Z}_{\mathrm{A}}(f)\boldsymbol{Z}_{\mathrm{A}}(f)^*\right) \\ & \times (\boldsymbol{Z}_{\mathrm{A}}(f)^*+R_{\mathrm{in}}\mathbf{I})^{-1}.\end{aligned} \tag{7}$$

After applying the Karush–Kuhn–Tucker (KKT) conditions on the quadratic constrained quadratic program (QCQP) [13], we get the following optimal beamforming vector as a function of the dissipated power, E, and the effective channel

$$\boldsymbol{b}(f) = \frac{\sqrt{E}}{||\boldsymbol{b}(f)^*\boldsymbol{G}^{-1}\boldsymbol{b}(f)||_2}\boldsymbol{G}^{-1}\boldsymbol{h}_{\mathrm{eff}}(f). \tag{8}$$

The beamforming vector in (8) is essential in finding the optimized spectral efficiency and helps in mitigating mutual coupling.

III. Antenna design

Extracting the impedance matrix $\boldsymbol{Z}_{\mathrm{A}}(f)$ solely depends on the designed antenna array simulated in HFSS. Therefore, we design a two-port physical antenna structure that satisfies a linear polarized antenna alignment. Fig. 2 illustrates the geometrical configurations of the designed two-port compact planar antenna. This parallel configuration is composed of two elliptical monopoles that generate a wideband frequency behavior [14].

Antenna parameter	Value (mm)	Parameter description
L_ℓ	27	length of substrate
W_ℓ	48	width of substrate$\|_{d=22\mathrm{mm}}$
R	6	ellipse major radius
D_l	2.6	length of the minor feed-line
F_ℓ	5.5	length of the major feed-line
L_t	7	length of the ground plane
H_t	24	width of the ground plane
d	12-22	inter-element spacing
D_w	2.5	width of the minor feed-line
F_w	3	width of the major feed-line

TABLE I: Antenna parameters.

The simulated parallel alignment is based on a $27\ \mathrm{mm} \times 48\ \mathrm{mm}$ FR4 substrate with $1.6\ \mathrm{mm}$ thickness and a dielectric constant of 4.4. The axial ratio is 1.3 and the major elliptical radius is $6\ \mathrm{mm}$. The feed-line of the antenna array is

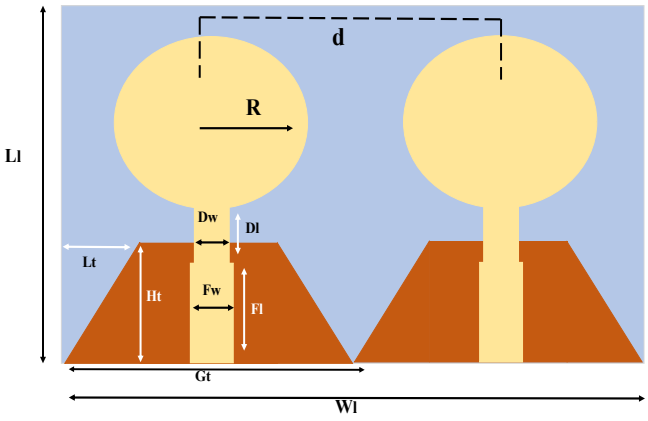

Fig. 2: Parallel antenna array structure composed of two elliptical monopoles and two trapezoidal ground planes.

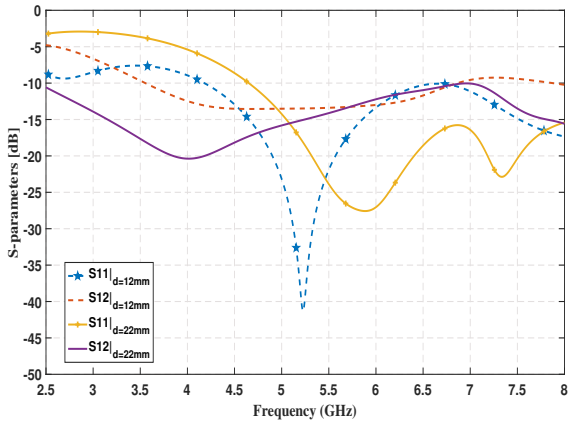

Fig. 3: S-parameters of the two-port antenna array structure at different inter-element spacing.

geometrically tapered to the elliptical monopole. The narrow feed-line, D_w is smoothly connected to a wider feed-line F_w. A truncated trapezoidal geometrical structure is used as the antenna ground plane.

To evaluate the impact of mutual coupling on the antenna's radiation pattern, we vary the inter-element spacing, d, of the parallel antenna array. If the inter-element spacing is $\leq \frac{\lambda}{2} = 18.7$ mm then the mutual coupling is high in the corresponding frequencies. Increasing the inter-element spacing to 22 mm allows us to compare the changes in the spectral efficiency.

The antenna array's S-parameters are presented in Fig. 3. The S-parameters are the conventional antenna's figures of merit that illustrate its circuit behavior. In fact, the S-parameters are directly related to the antenna's impedance matrix by the transformation $\boldsymbol{S} = (\boldsymbol{Z}_{\mathrm{A}}/50\Omega - \mathbf{I})(\boldsymbol{Z}_{\mathrm{A}}/50\Omega + \mathbf{I})^{-1}$. To capture the region of operation and the regions with the highest mutual coupling, we vary the spacing between the elements and capture the S-parameter response. We extract the reflection coefficients, e.g. S_{11}, from the HFSS simulation. Proper antenna operation requires conventionally that S_{11} is below -10 dB. Accordingly, the designed antenna operates between 4.14-8GHz when the inter-element spacing is 12 mm. The antenna array's radiation pattern in Fig. 4 is evaluated at $f = 8$GHz and $d = 22$ mm.

Furthermore, the mutual coupling indicator, S_{12}, is also plotted in Fig. 3 at different inter-element spacing $d \in \{12, 22\}$ mm. Antenna arrays that mitigate the mutual coupling effects maintain an S_{12}<-15 dB. In our design, however, we are accounting for mutual coupling and focus on the frequency regions where it is severe. Therefore, we focus on the regions that have an S_{12}>-15 dB$|_{d=12\ \mathrm{mm}}$ and S_{12}>-15 dB$|_{d=22\ \mathrm{mm}}$. These regions will be important when computing the optimal beamforming vector that essentially depends on the coupling effects to achieve an improved spectral efficiency.

IV. Numerical Results

In this section, we evaluate the spectral efficiency of the two element MISO system using the two different power

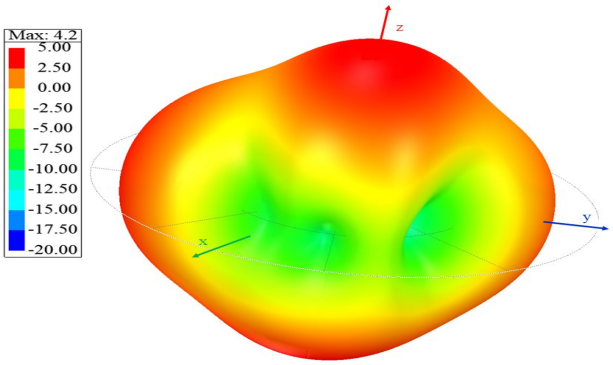

Fig. 4: Realized antenna gain at $f = 8\mathrm{GHz}|_{d=22\mathrm{mm}}$.

constraints for the beamformer design. We consider the angle of departures, $\theta = 0$, which mimics an end-fire configuration and $\theta = \frac{\pi}{2}$ i.e. broadside direction. We vary the inter-element spacing $d \in \{12, 22\}$ mm to visualize the impact of mutual coupling. We begin our analysis with a Line-of-Sigh (LoS) channel model. The propagation channel, $\boldsymbol{h}_{\mathrm{prop,LoS}}(f)$, also considers the transmit antenna's radiation pattern $\mathcal{P}(\theta)$ (with 2D beamforming) and is given by (with isotropic Rx antenna)

$$\boldsymbol{h}_{\mathrm{prop,LoS}}(f) = \frac{\lambda}{4\pi D} \begin{bmatrix} 1 \\ e^{-j2\pi \frac{d}{\lambda} \cos\theta} \end{bmatrix} \sqrt{\mathcal{P}(\theta)}, \tag{9}$$

where $D = 2$ km is the distance between the Tx and Rx antennas. This path-loss model is characterized by the simplified Friis transmission equation [14].

Our objective is to maximize the spectral efficiency. So we define the frequency-dependent SNR as

$$\mathrm{SNR}(f) = \frac{|\boldsymbol{h}_{\mathrm{eff}}(f)^{\mathrm{T}} \boldsymbol{b}(f)|^2}{N_0 N_{\mathrm{F}}}, \tag{10}$$

where $N_0 = B_k k_{\mathrm{b}} T$ and k_{b} is the Boltzman constant, $T = 290$ K, $N_{\mathrm{F}} = 5$dB is the noise figure of the receiver, and $E = 250$ mW/20 MHz. Accordingly, the spectral efficiency is

$$C(f) = \log_2(1 + \mathrm{SNR}(f)). \tag{11}$$

We plot the spectral efficiency of the two beamformers at different inter-element spacing and compare them to the performance of a perfectly matched single omni-directional antenna (Friis curve), i.e.,

$$C_{\text{Friis}}(f) = \log_2\left(1 + \alpha_c(f)\frac{E}{N_0 N_{\text{F}}}\right), \tag{12}$$

where $\alpha_c(f)$ is the frequency-dependent channel path-loss. Fig. 5 shows that the computed optimal beamformer, under fixed dissipated power, has better spectral efficiency in comparison to the $L2$ norm constraint, since source currents are not limited. Furthermore, since the source currents are not directly limited, the presence of mutual coupling ($d = 12$ mm) results partially in higher achievable rates for both beamformers. Tighter spacing might be beneficial for certain frequency bands, but can also lead to some performance degradation for other frequencies. Additional measures can be taken to improve the achievable rate of the beamformer constraint over the $L2$ norm. One of these approaches motivates the use of multiport matching networks [8].

V. Conclusion

In this paper, we designed a two-port wideband antenna array by means of full-wave simulation in HFSS. Using this antenna array, we evaluated the spectral efficiency of a MISO system in the broadband regime. The beamforming vectors are optimized under different power constraints while accounting for the effects of mutual coupling. The results showed that the optimal beamforming vector strongly depends on the type of power constraints and the degree of mutual coupling in the antennas. Potential venues for our future work considers different channel propagation models, a larger number of antennas, and advanced matching techniques to further mitigate mutual coupling effects.

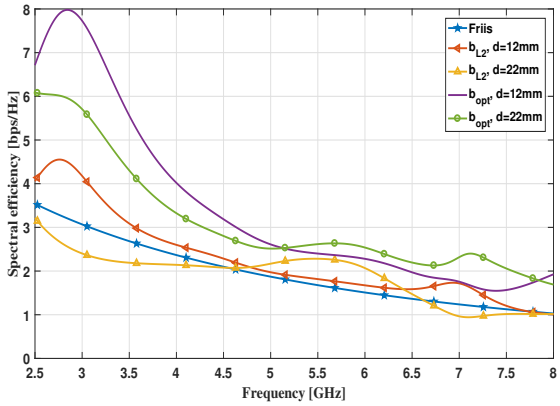

(a) Spectral efficiency at $\theta = 0$.

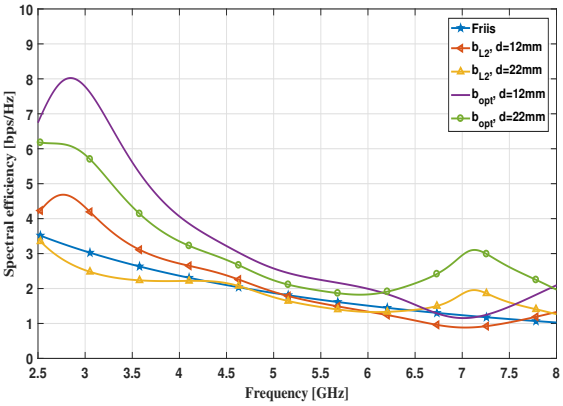

(b) Spectral efficiency at $\theta = \frac{\pi}{2}$.

Fig. 5: Spectral efficiency of the antenna array when using the optimal beamforming vector, b_{opt}, vs. that obtained from the b_{L2} norm constraint. The spectral efficiency is evaluated at different inter-element spacing.

VI. Acknowledgement

This material is based upon work supported in part by the National Science Foundation under Grant No. ECCS-1711702 and CNS-1731658.

References

[1] M. Sakai, K. Kamohara, H. Iura, H. Nishimoto, K. Ishioka, Y. Murata, M. Yamamoto, A. Okazaki, N. Nonaka, S. Suyama, J. Mashino, A. Okamura, and Y. Okumura, "Experimental field trials on MU-MIMO transmissions for high SHF wide-band massive MIMO in 5G," *IEEE Transactions on Wireless Communications*, vol. 19, no. 4, pp. 2196–2207, 2020.

[2] R. Vaughan and J. B. Andersen, *Channels, Propagation and Antennas for Mobile Communications*. Inst. Elect. Eng, 2003.

[3] T. Svantesson and A. Ranheim, "Mutual coupling effects on the capacity of multielement antenna systems," in *2001 IEEE International Conference on Acoustics, Speech, and Signal Processing. Proceedings*, vol. 4, 2001, pp. 2485–2488 vol.4.

[4] M. K. Ozdemir, E. Arvas, and H. Arslan, "Dynamics of spatial correlation and implications on MIMO systems," *IEEE Communications Magazine*, vol. 42, no. 6, pp. S14–S19, 2004.

[5] Y. Cheng, X. Ding, W. Shao, and B. Wang, "Reduction of Mutual Coupling Between Patch Antennas Using a Polarization-Conversion Isolator," *IEEE Antennas and Wireless Propagation Letters*, vol. 16, pp. 1257–1260, 2017.

[6] S. Zhang and G. F. Pedersen, "Mutual Coupling Reduction for UWB MIMO Antennas with a Wideband Neutralization Line," *IEEE Antennas and Wireless Propagation Letters*, vol. 15, pp. 166–169, 2016.

[7] N. Ma and H. Zhao, "Reduction of the mutual coupling between aperture coupled microstrip patch antennas using EBG structure," in *2014 IEEE International Wireless Symposium (IWS 2014)*, 2014, pp. 1–4.

[8] M. T. Ivrlač and J. A. Nossek, "Toward a Circuit Theory of Communication," *IEEE Trans. on Circuits and Systems I: Regular Papers*, vol. 57, no. 7, pp. 1663–1683, July 2010.

[9] R. W. Heath Jr. and A. Lozano, *Foundations of MIMO Communication*. Cambridge University Press, 2018.

[10] J. W. Wallace and M. A. Jensen, "Mutual coupling in MIMO wireless systems: a rigorous network theory analysis," *IEEE Trans. on Wireless Comm.*, vol. 3, no. 4, pp. 1317–1325, July 2004.

[11] S. Saab, A. Mezghani, and R. W. Heath, "Capacity Based Analysis of a Wideband SIMO System in the Presence of Mutual Coupling," in *2019 IEEE Global Communications Conference*, 2019, pp. 1–6.

[12] *3D Electromagnetic Field Simulator for RF and Wireless Design*, ANSYS, 2018, [Online]. Available: https://www.ansys.com/products/electronics/ansys-hfss.

[13] S. Boyd, S. P. Boyd, and L. Vandenberghe, *Convex optimization*. Cambridge university press, 2004.

[14] C. A. Balanis, *Antenna theory: analysis and design*, 2nd ed. Hoboken, NJ, USA: Wiley, 1997.